The Dissipation of Trapped Lee Waves. Part II: The Relative Importance of the Boundary Layer and the Stratosphere

MATTHEW O. G. HILLS

Department of Atmospheric Sciences, University of Utah, Salt Lake City, Utah

DALE R. DURRAN AND PETER N. BLOSSEY

Department of Atmospheric Sciences, University of Washington, Seattle, Washington

(Manuscript received 24 June 2015, in final form 23 October 2015)

ABSTRACT

Decaying trapped waves exert a drag on the large-scale flow. The two most studied mechanisms for such decay are boundary layer dissipation and leakage into the stratosphere. If the waves dissipate in the boundary layer, they exert a drag near the surface, whereas, if they leak into the stratosphere, the drag is exerted at the level where the waves dissipate aloft. Although each of these decay mechanisms has been studied in isolation, their relative importance has not been previously assessed.

Here, numerical simulations are conducted showing that the relative strength of these two mechanisms depends on the details of the environment supporting the waves. During actual trapped-wave events, the environment often includes elevated inversions and strong winds aloft. Such conditions tend to favor leakage into the stratosphere, although boundary layer dissipation becomes nonnegligible in cases with shorter resonant wavelengths and higher tropopause heights. In contrast, idealized two-layer profiles with constant wind speeds and high static stability beneath a less stable upper troposphere support lee waves that are much more susceptible to boundary dissipation and relatively unaffected by the presence of a stratosphere. One reason that trapped waves in the two-layer case do not leak much energy upward is that the resonant wavelength is greatly reduced in the presence of surface friction. This reduction in wavelength is well predicted by the linear inviscid equations if the basic-state profile is modified a posteriori to include the shallow ground-based shear layer generated by surface friction.

1. Introduction

Trapped lee waves are a category of mountain wave that extend downstream of terrain, with the bulk of their energy contained within a lower-tropospheric resonant wave duct. The distance over which the lee-wave train extends depends upon several factors, including the roughness of the underlying surface, the efficiency with which wave energy can leak upward through the stratosphere, the steadiness of the flow, and the degree to which energy is removed by lateral dispersion from three-dimensional terrain. In this paper, we will compare the relative efficiency of two possible dissipation mechanisms, surface friction and stratospheric leakage, which have been the subject of most previous studies.

Bretherton (1969) estimated the drag produced by the turbulent absorption of lee waves, either in an elevated layer or at the surface. The drag from trapped lee waves can be a significant fraction of the total gravity wave drag and thus has an important impact on the large-scale weather and climate (Durran 1995; Georgelin and Lott 2001; Broad 2002; Stiperski and Grubišić 2011; Teixeira et al. 2013). The influence of dissipating trapped waves on the mean flow depends, in part, on the level at which the dissipation occurs. If trapped waves are absorbed in the boundary layer, this drag will be exerted at low levels, whereas, if they leak upward into the stratosphere, the drag will be exerted at the level at which they dissipate in the upper atmosphere.

Recent research has shown that lee waves can be effectively absorbed by boundary layer processes. Smith et al. (2002) presented observations of lee-wave

Corresponding author address: Matthew O. G. Hills, Department of Atmospheric Sciences, University of Utah, 135 S 1460 E, Rm. 819, Salt Lake City, UT 84112-0110.
E-mail: matt.hills@utah.edu

DOI: 10.1175/JAS-D-15-0175.1

absorption at a critical level in a stagnant layer in the lee of Mont Blanc. In the absence of a critical layer, increasing surface roughness has been shown to increase the rate of downstream decay of the lee-wave train (Smith et al. 2006; Jiang et al. 2006). These studies of the influence of surface friction did not, however, consider environmental conditions where the lee waves could potentially leak energy upward through the stratosphere. Such upward energy leakage has been observed in several field campaigns (Vergeiner 1971; Brown 1983; Shutts 1992; Georgelin and Lott 2001). Durran et al. (2015, hereafter DHB15) obtained solutions to the vertical structure equation for linear partially trapped waves showing that upward leakage of energy through the stratosphere can be an effective mechanism for the downstream decay of trapped lee waves. The rate at which energy leaked upward was strongly dependent on the fraction of the trapped-wave amplitude that penetrated upward to the tropopause. Higher rates of leakage were favored by longer resonant wavelengths and lower tropopause heights. Leakage was often significant in the trapped-wave environments with elevated inversions and strong upper-tropospheric winds typically found during actual atmospheric events. On the other hand, the importance of upward leakage was highly variable among cases where the stratosphere capped idealized profiles, with constant wind speed and two layers of uniform static stability in the troposphere.

The aim of this paper is to compare the roles of the stratosphere and the boundary layer in causing downstream trapped-wave decay. Our primary focus will be on stratospheres with typical near-isothermal static stability and surface roughnesses representative of the ocean or open shrublands. Section 2 outlines the numerical model used for our study. Profiles with uniform wind speed and two-layer tropospheric static stability structures are considered in section 3. Profiles in which the waves are trapped by strong upper-level winds and low-level stability concentrated in elevated inversions are examined in section 4. The conclusions are presented in section 5.

2. Model description

All simulations are performed with an updated version of the Durran and Klemp (1983) mesoscale model (meso12) used recently in dry and moist mountain-wave simulations (Hills and Durran 2012, 2014). The model is fully nonlinear, nonhydrostatic, and compressible, and it employs terrain-following coordinates. The two-dimensional dry simulations in this paper simplify the dynamics through use of the compressible Boussinesq approximation, which neglects the influence of density changes with height but allows the pressure to respond to convergence or divergence in the velocity field. Expressed without the terrain transformed coordinates for simplicity, the model solves

$$\frac{Du}{Dt} - fv + \frac{\partial P}{\partial x} = D_u, \tag{1}$$

$$\frac{Dv}{Dt} + fu = D_v, \tag{2}$$

$$\frac{Dw}{Dt} + \frac{\partial P}{\partial z} = g\left(\frac{\theta - \overline{\theta}}{\theta_0}\right) + D_w, \tag{3}$$

$$\frac{D\theta}{Dt} = D_\theta, \quad \text{and} \tag{4}$$

$$\frac{\partial P}{\partial t} + c_{s_0}^2\left(\frac{\partial u}{\partial x} + \frac{\partial w}{\partial z}\right) = 0, \tag{5}$$

where

$$\frac{D}{Dt} = \frac{\partial}{\partial t} + u\frac{\partial}{\partial x} + w\frac{\partial}{\partial z}. \tag{6}$$

In the above, (u, v, w) are the velocity components in the cross-ridge x, along-ridge y, and vertical z directions; g is gravity; θ is potential temperature; $\overline{\theta}(z)$ is the initial potential temperature profile; P is the Boussinesq pressure perturbation about the pressure field in hydrostatic balance with $\overline{\theta}$; $\theta_0 = 290\,\mathrm{K}$ is a constant temperature nominally at the surface; c_{s_0} is the speed of sound ($300\,\mathrm{m\,s^{-1}}$); and f is the Coriolis parameter set to a representative midlatitude value of $1 \times 10^{-4}\,\mathrm{s^{-1}}$ in those runs with surface friction and is set to zero otherwise. The turbulent subgrid-scale fluxes of momentum D_u, D_v, D_w, and D_θ are parameterized following Lilly (1962) and are described further in appendix A.

The planetary boundary layer is incorporated in the model by a parameterization based on Blackadar's first-order-closure scheme described by Zhang and Anthes (1982) and used by Gaberšek and Durran (2006) (appendix B describes the simplified version of this parameterization used by meso12). Differences in surface friction are imposed by adjusting the roughness length z_0, with particular emphasis on values representative of an ocean surface ($z_0 = 0.0001\,\mathrm{m}$) or moderately open country ($z_0 = 0.1\,\mathrm{m}$) (Wieringa 1992). As such, these values provide a contrast between lee waves extending away from a ridge over typical ocean and land surfaces. Heat fluxes are neglected, both to focus on a limited parameter space and because of the substantial differences in sensible heat transfer that might be expected beneath lee waves over the oceans and the land.

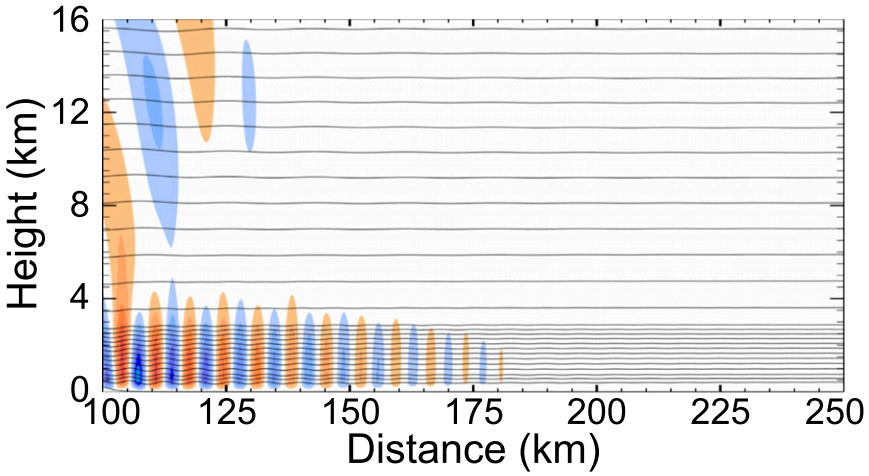

FIG. 1. Cross section of the vertical velocity w (color fill at 0.25 m s^{-1} intervals; no fill for $-0.25 < w < 0.25$ m s^{-1}), and potential temperature isentropes (black lines; 4-K interval) for profile 1 with $z_0 = 0.1$ m.

The horizontal grid spacing in all simulations is 250 m. The vertical coordinate is stretched to allow high resolution in the lower atmosphere such that $\Delta z = 30$ m at heights below 2 km, which gradually stretches to 100 m over the next 4 km and remains fixed at 100 m above 6 km to the model top at 25 km. At the rigid upper boundary, wave reflections are prevented using the Klemp–Durran–Bougeault (KDB) radiation condition (Bougeault 1983; Klemp and Durran 1983). Periodic lateral boundaries are used, and the 5-h simulation time is short enough to prevent any downstream disturbances from wrapping around the domain and affecting the incoming flow. Initial transients generated by surface friction in the low-level horizontal velocity and potential temperature fields have become almost completely steady by the end of the simulation. A split–time step method is used to integrate the model equations, with the fast-moving sound waves evaluated on a smaller time step (0.2 s) which allows the model to remain stable while using a relatively large time step (2.0 s) for the bulk of the dynamics. All figures show results at a time of 5 h when the wave trains have reached steady state in all simulations.

Terrain at the lower boundary is represented by a Witch of Agnesi profile:

$$h(x) = \frac{h_0}{1 + [(x - x_0)/a]^2}. \tag{7}$$

In all simulations, the ridge is centered at $x_0 = 100$ km, although its height h_0 and half-width a vary between simulations in order to ensure a linear mountain-wave response; their values will be noted in each of the following sections. The vertical profiles of stability and cross-mountain wind speed vary significantly throughout this study and will be discussed in each of the following sections. When possible, the names of the vertical profiles match those used in DHB15.

3. Constant N and U

a. *Profile 1: Short resonant wavelengths*

We first consider the two-layer environmental profile used by Jiang et al. (2006) to investigate the influence of surface friction on trapped waves. This profile [also used in Doyle and Durran (2002)] contains a 3-km-deep lower layer with $N = 0.025$ s^{-1} and $N = 0.01$ s^{-1} above this; $u = 25$ m s^{-1} at all levels. Figure 1 shows the steady solution obtained from a simulation of this profile flowing over a mountain of the form of (7) with $a = 2.5$ km and $h_0 = 200$ m, with $z_0 = 0.1$ m. In agreement with the identical simulation in Jiang et al. (2006), the resonant horizontal wavelength is $\lambda = 7.5$ km, and the waves decay rapidly with distance downstream and have little vertical extent.[1] DHB15 showed that, in the inviscid case, for which the resonant wavelength is marginally longer ($\lambda = 9.3$ km), adding a stratosphere as a third layer beginning at $z = 10$ km has negligible impact on the wave amplitude downstream because the waves decay so rapidly with height through the upper troposphere that little energy reaches the stratosphere. As noted in DHB15, when the Scorer parameter is a constant l_u in the upper-troposphere layer, the e-folding scale for the vertical decay of trapped waves in that layer is

[1] All resonant wavelengths discussed in this paper are in the horizontal.

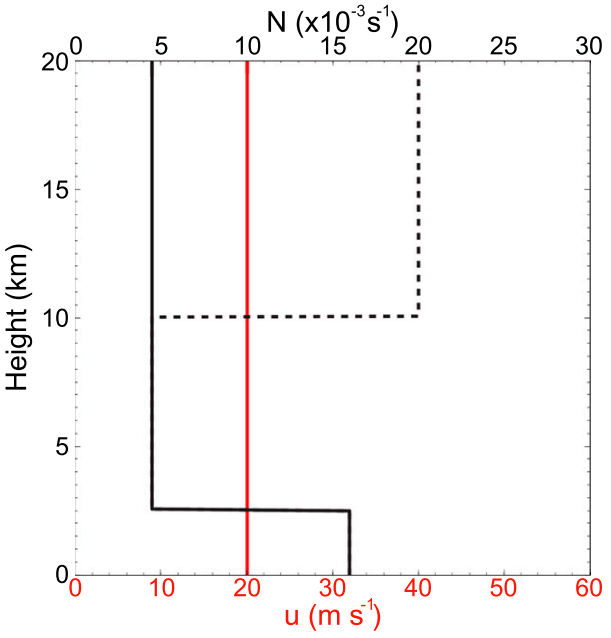

FIG. 2. Environment for profile 2: cross-mountain wind speed (red; lower axis) and Brunt–Väisälä frequency (black; upper axis). The solid (dashed) lines show the no-stratosphere (stratosphere) cases.

$$\left[\left(\frac{2\pi}{\lambda}\right)^2 - l_u^2\right]^{-1/2}, \tag{8}$$

which decreases as the resonant wavelength decreases. Given that the resonant wavelength decreased in Fig. 1 relative to that in the inviscid case, it is not surprising that additional simulations (not shown) confirm that boundary layer processes are much more effective than leakage into the stratosphere in producing downstream decay when the environmental conditions are given by profile 1.

b. *Profile 2: Long resonant wavelengths*

Ralph et al. (1997) compiled observations of 24 trapped-wave events and noted their horizontal wavelengths ranged between 8.3 and 28.6 km; the average horizontal wavelength was 15.8 ± 4.5 km. The profile-1 waves that develop in the presence of surface friction are shorter than all those in the Ralph et al. (1997) sample. Does stratospheric leakage become a more effective decay mechanism than surface friction in simple two-layer atmospheres that support longer resonant wavelengths? Figure 2 shows the vertical structure of the wind speed and Brunt–Väisälä frequency for profile 2, in which the static stability is $N = 0.016\,\mathrm{s}^{-1}$ throughout a 2.5-km-deep lower layer, topped by a layer in which $N = 0.0045\,\mathrm{s}^{-1}$. When a stratosphere is present, N increases to $0.02\,\mathrm{s}^{-1}$ above a height of 10 km. At all heights, u is $20\,\mathrm{m\,s}^{-1}$. The eigenvalue analysis in DHB15 gives a 20.5-km resonant wavelength for profile 2 without surface friction or a stratosphere.

Figure 3 shows the vertical velocities and isentropes for simulations with and without stratospheres and three different surface conditions. The terrain parameters in (7) for these simulations are $h_0 = 100$ m and $a = 2.5$ km. To facilitate their comparison, the vertical velocities in all panels are normalized by the maximum w within the first updraft in the lee of the terrain. Figure 3a illustrates the free-slip situation with no stratosphere. In good agreement with the linear model, the resonant wavelength is 20.8 km. Note that, in this free-slip case, the vertical extent of the waves is much greater than those in profile 1 (Fig. 1). When the stratosphere is present but there is no surface friction, profile-2 waves decay gradually downstream; slightly less than half of the initial energy is removed 150 km downstream (Fig. 3b).

The decay produced solely by stratospheric leakage may be compared to that generated solely by surface friction for cases with $z_0 = 0.0001$ m (Fig. 3c) or $z_0 = 0.1$ m (Fig. 3d). Much stronger downstream decay occurs in both of these simulations, with essentially all wave activity dissipated 50 km downstream of the crest when $z_0 = 0.1$ m. Surface friction also produces a strong reduction in horizontal wavelength as the roughness length is increased. From 20.8 km in the free-slip case, λ is almost halved to 12.9 km when $z_0 = 0.0001$ m, and it further decreases to 10.4 km as z_0 is increased to 0.1 m. Jiang et al. (2006) noted the resonant wavelength in their simulations of completely trapped waves decreased in the presence of a boundary layer, and they demonstrated theoretically that absorption of the downward-propagating component of the trapped wave did not have a first-order impact on the resonant wavelength. As will be discussed in the conclusions, the reduction in λ primarily occurs because of the reduced low-level wind speeds in the boundary layer, and this change is accurately captured if linear theory is applied to evaluate λ for a basic-state profile modified to include the surface-based shear layer. Accompanying this reduction in the horizontal wavelength is a similarly large reduction in the scale over which the trapped waves decay in the vertical.

The combined effects of stratospheric leakage and surface friction on the waves are shown in Figs. 3e,f. For both values of z_0 the rate of downstream decay is almost unchanged by the presence of the stratosphere. As for profile 1, boundary layer absorption is the dominant, and essentially exclusive, decay mechanism for the trapped waves supported by profile 2.

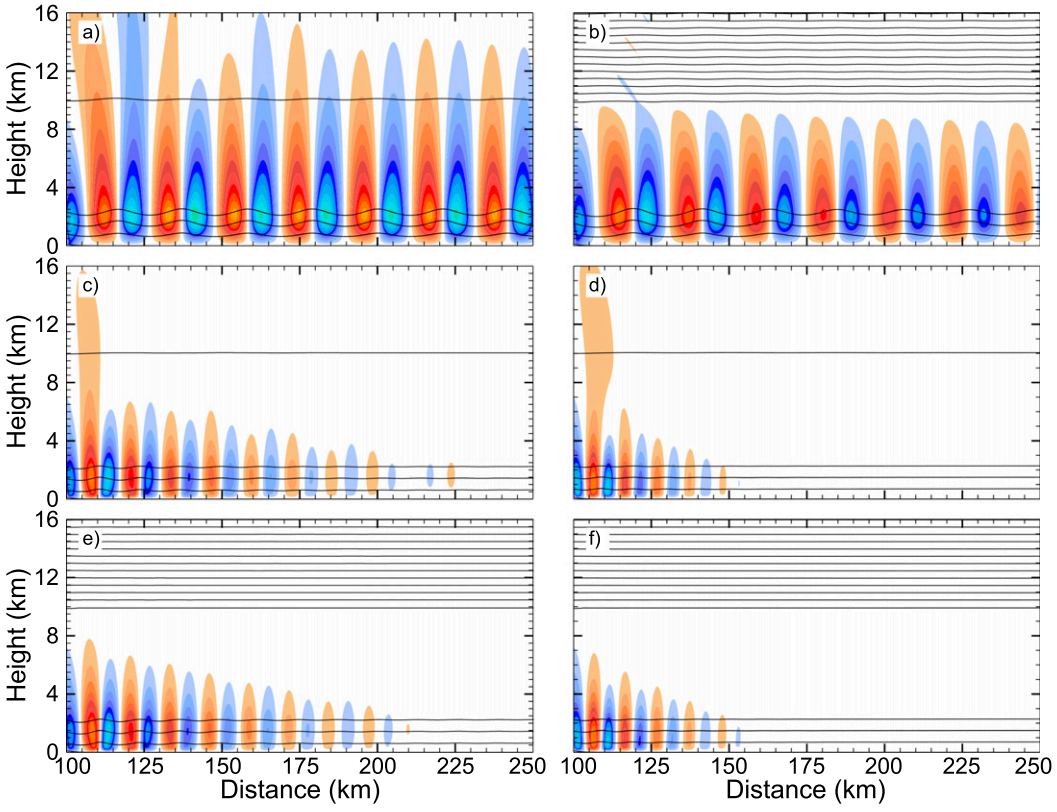

FIG. 3. Cross section of the normalized vertical velocity (color fill; 0.1 intervals; no fill for $-0.1 < w < 0.1\,\mathrm{m\,s^{-1}}$) and isentropes of potential temperature (black; 6-K interval) for profile 2: (a) free slip, $N_s = 0.0045\,\mathrm{s^{-1}}$; (b) free slip, $N_s = 0.02\,\mathrm{s^{-1}}$; (c) $z_0 = 0.0001$ m, $N_s = 0.0045\,\mathrm{s^{-1}}$; (d) $z_0 = 0.1$ m, $N_s = 0.0045\,\mathrm{s^{-1}}$; (e) $z_0 = 0.0001$ m, $N_s = 0.02\,\mathrm{s^{-1}}$; and (f) $z_0 = 0.1$ m, $N_s = 0.02\,\mathrm{s^{-1}}$.

c. *Profile 2 decay rates*

Figure 4 quantifies the rate of downstream decay for simulations forced using profile 2 with a range of different stratospheric stabilities and surface roughnesses. Decay is calculated as the decrease in wave amplitude over one horizontal wavelength, as averaged across the first 5 wavelengths at $z = 3$ km. First consider the no-stratosphere, variable-z_0 simulations illustrated in Figs. 3a,c,d. The associated decay rates are along the left axis. The strong increase in downstream decay that occurs when switching from a free-slip condition to a boundary layer is readily apparent. There is an approximately linear increase in the percentage rate of decay with $\ln(z_0)$.

The rate of downstream decay generated by upward leakage due to the stratosphere in the free-slip profile-2 situation is shown by the black line in Fig. 4. The form of this curve is similar to that obtained using linear theory in DHB15 (see their Fig. 4a), with the maximum decay of 18% here agreeing well with the 16% in the linear model. A sharp increase in the rate of decay occurs across the threshold value of $N_s = 0.007\,\mathrm{s^{-1}}$, and there is a decrease in the rate of decay to approximately 8% per wavelength at $N_s = 0.03\,\mathrm{s^{-1}}$, compared to 7% in the linear model. The agreement between the decay rates calculated as solutions to the eigenvalue problem in DHB15 and the decay rates from the full numerical simulations adds confidence to our results.

Despite the stratosphere alone being capable of producing an 18% decay rate in the free-slip case, the stratospheric stability has essentially no influence on the decay rate for all nonzero values of z_0 considered in Fig. 4.[2] This somewhat unintuitive result may be better understood by considering the structure of the wave field in the two-layer situation with and without surface friction. Compare Figs. 3a and 3c. In the free-slip situation, a significant fraction of the total wave amplitude

[2] There is a slight reduction in the rate of decay with a stratosphere for the short roughness length simulations at low values of N_s, although we consider this to be an artifact of the slight reduction in amplitude in the lee of the terrain as the stratosphere is introduced (because of stronger downslope flow pushing the first updraft farther downstream), rather than an inherent decay property.

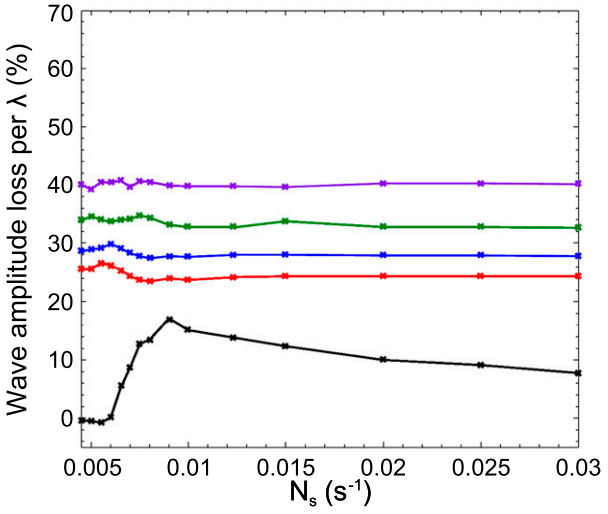

FIG. 4. Percentage loss of wave amplitude at $z = 3$ km per horizontal wavelength downstream using profile 2: free slip (black); $z_0 = 0.0001$ m (red); $z_0 = 0.001$ m (blue); $z_0 = 0.01$ m (green); and $z_0 = 0.1$ m (purple).

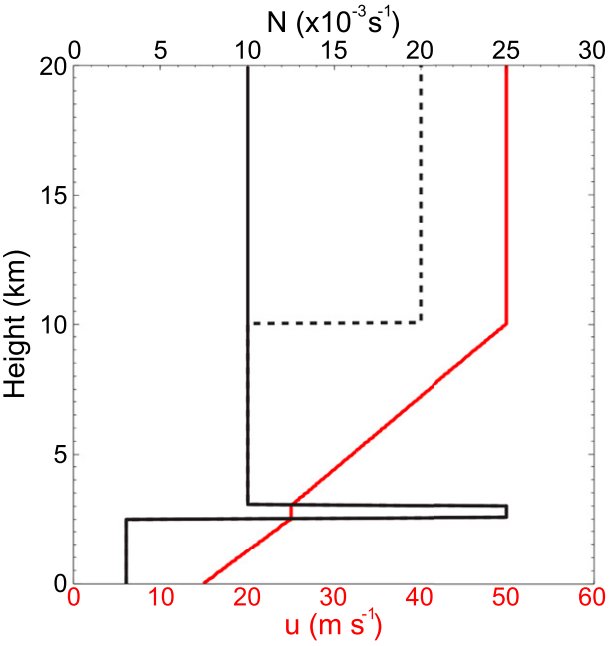

FIG. 5. As in Fig. 2, but for profile 3a.

reaches the height of the tropopause, but with surface friction this is prevented, the waves decay almost entirely before penetrating halfway through the troposphere, and there is little signal left to leak upward through the stratosphere.

4. Forward wind shear and elevated inversion

a. *Profile 3a*

In the atmosphere, trapped waves often occur when the wind speed increases with height throughout the troposphere and the low-level static stability is concentrated in an elevated inversion. Profile 3a is such a case; it is representative of the conditions observed over the Intermountain West of the United States on 17 March 2005—a day that was characterized by a widespread and long-lived trapped-wave event stretching from California to Colorado. As plotted in Fig. 5, $N = 0.003\,\mathrm{s}^{-1}$ below $z = 2.5$ km, there is an inversion with $N = 0.025\,\mathrm{s}^{-1}$ in the layer $2.5 \le z \le 3.0$ km, and $N = 0.01\,\mathrm{s}^{-1}$ above 3 km. Zonal wind speeds increase from 15 to $25\,\mathrm{m\,s}^{-1}$ and from 25 to $50\,\mathrm{m\,s}^{-1}$ below and above the inversion, respectively.[3] The tropopause, when present, is at $z = 10$ km. The terrain for these simulations is given by (7) with $h_0 = 250$ m and $a = 2$ km; the vertical velocity is again normalized by the maximum w within the first updraft in the lee of the terrain.

[3] Profile 3a differs only from profile 3 of DHB15 in that there is no wind shear across the elevated inversion.

Figure 6a shows the structure of the trapped waves supported by profile 3a with no stratosphere and a free-slip lower boundary. Although they have a 21.8-km resonant wavelength similar to that in Fig. 3a, the strong upper-tropospheric winds in profile 3a greatly increase the vertical scale over which the waves decay. The influence of the stratosphere, with $N_s = 0.02\,\mathrm{s}^{-1}$, is shown for free-slip conditions in Fig. 6b. Rapid decay of the solution is evident, with the wave train reduced to approximately 20% of its initial amplitude 75 km downstream from the crest and all waves removed by 125 km. The upstream tilt of these waves in the stratosphere is clearly visible. Simulations of profile 3a with no stratosphere and with $z_0 = 0.0001$ m or $z_0 = 0.1$ m are shown in Figs. 6c and 6d, respectively. As previously, when the surface roughness is increased, there is an increase in the rate of downstream decay of the wave train. In the $z_0 = 0.1$ m case, the wave amplitude is reduced to approximately 20% of its initial amplitude 125 km downstream of the crest, but this decay is significantly weaker than that in the free-slip case with a stratosphere (Fig. 6b).

In contrast to the situation with profile 2, surface friction produces only a small reduction in the 21.8-km wavelength of the trapped waves supported by profile 3a. The resonant wavelength drops to 19.8 km when $z_0 = 0.0001$ m and 18.7 km when $z_0 = 0.1$ m. Consequently, the vertical extent of the trapped waves in Figs. 6c,d is only minimally reduced relative to the free-slip case. Because a significant fraction of the maximum wave amplitude remains at $z = 10$ km, the

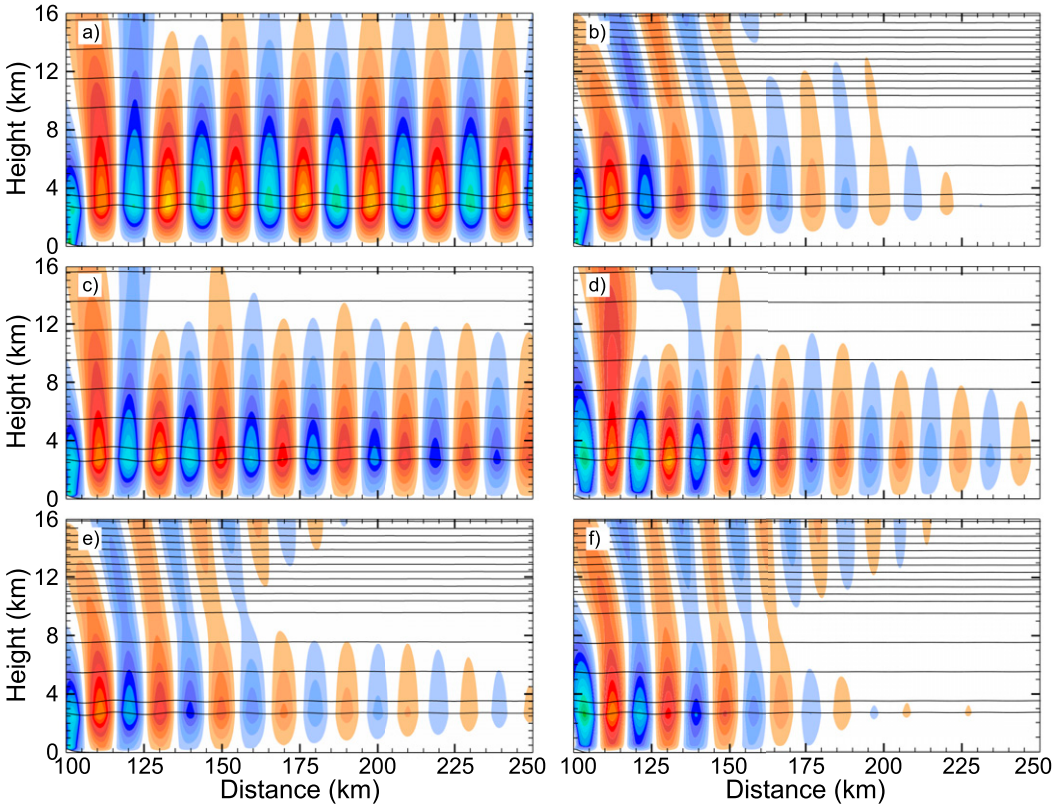

FIG. 6. As in Fig. 3, but for profile 3a: (a) free slip, $N_s = 0.01\,\mathrm{s}^{-1}$; (b) free slip, $N_s = 0.02\,\mathrm{s}^{-1}$; (c) $z_0 = 0.0001$ m, $N_s = 0.01\,\mathrm{s}^{-1}$; (d) $z_0 = 0.1$ m, $N_s = 0.01\,\mathrm{s}^{-1}$; (e) $z_0 = 0.0001$ m, $N_s = 0.02\,\mathrm{s}^{-1}$; and (f) $z_0 = 0.1$ m, $N_s = 0.02\,\mathrm{s}^{-1}$.

simulations with both surface friction and a stratosphere, plotted in Figs. 6e and 6f, show much more rapid decay than those with surface friction alone. The most rapid decay occurs when the stratosphere is present and the surface roughness is large ($z_0 = 0.1$ m). Counterintuitively, the combination of weak surface friction ($z_0 = 0.0001$ m) and a stratosphere (Fig. 6e) produces weaker decay than that from the stratosphere alone (Fig. 6b). Weak surface friction does not directly generate much decay (Fig. 6c), but relative to the free-slip case, it still shortens the horizontal wavelength and the vertical extent of the trapped waves, thereby reducing the leakage of energy through the stratosphere.

The percentage loss of wave amplitude per wavelength in the free-slip case is plotted as a function of stratospheric stability by the black line in Fig. 7. For small values of N_s, there is essentially no downstream decay. A rapid increase in the rate of decay occurs for stabilities beyond the $N_s = 0.015\,\mathrm{s}^{-1}$ threshold for leakage into the stratosphere. The maximum rate of decay occurs for $N_s = 0.023\,\mathrm{s}^{-1}$, with approximately 51% of the wave amplitude lost as a result of stratospheric leakage per wavelength downstream. Turning to the cases with surface friction, for any given value of N_s, increasing z_0 increases the rate of downstream decay, but, for $0.017 \le N_s \le 0.024\,\mathrm{s}^{-1}$, the free-slip simulations exhibit more rapid decay than those

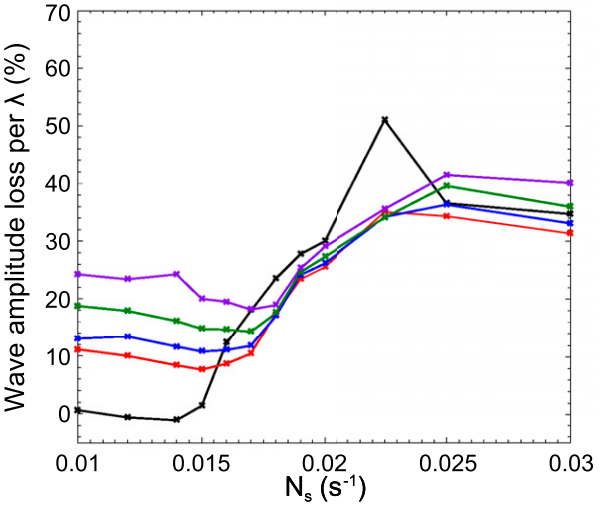

FIG. 7. Percentage loss of wave amplitude at $z = 3$ km per horizontal wavelength downstream using profile 3a: free slip (black); $z_0 = 0.0001$ m (red); $z_0 = 0.001$ m (blue); $z_0 = 0.01$ m (green); and $z_0 = 0.1$ m (purple).

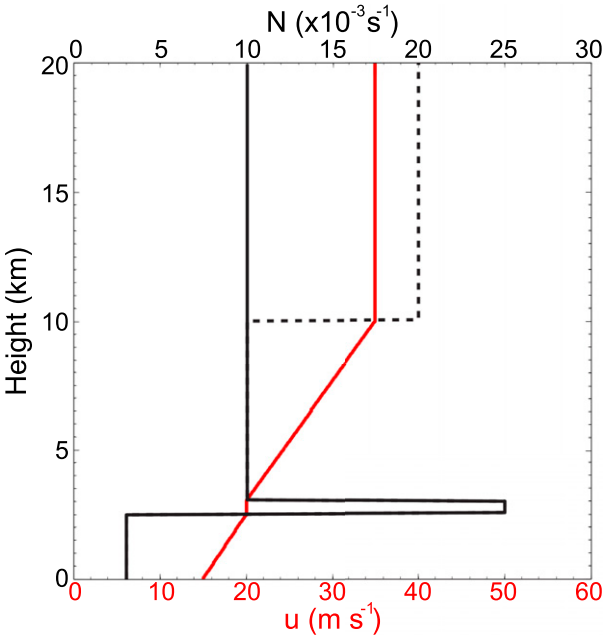

FIG. 8. As in Fig. 3, but for profile 3b.

generated by all the roughness values we tested. The maximum rate of decay due to the stratosphere alone is approximately 2 times stronger than that due to the roughest surface alone (a 24% loss per wavelength when $z_0 = 0.1$ m with no stratosphere present). For profile 3a, the stratosphere is a significantly stronger potential source of downstream decay than the boundary layer.

b. *Profile 3b*

The trapped wavelengths supported by profile 3a are toward the long end of the range of observed wavelengths in the cases compiled by Ralph et al. (1997). At least for the cases considered so far, waves with longer resonant wavelengths tend to decay more slowly with height and to be more susceptible to decay through the leakage into the stratosphere. Profile 3b allows us to examine the behavior of waves with resonant wavelengths shorter than the 15.8-km average wavelength in the set compiled by Ralph et al. (1997). Figure 8 plots the vertical profiles of u and N for profile 3b. The tropospheric stability structure is identical to that in profile 3a, with an elevated inversion in the layer $2.5 \le z \le 3.0$ km. The stratospheric stability is again $N_s = 0.02\,\mathrm{s}^{-1}$, but tropopause heights of $z_T = 9$ and 10 km will both be investigated. The shear is reduced, relative to profile 3a, such that the winds increase linearly from 15 to $20\,\mathrm{s}^{-1}$ between the surface and the bottom of the inversion and from 20 to $35\,\mathrm{m\,s}^{-1}$ between the top of the inversion and the tropopause (at either 9 or 10 km). The terrain for these simulations is given by (7) with $h_0 = 250$ m and $a = 2$ km; the vertical velocity is again normalized by the maximum w within the first updraft in the lee of the terrain.

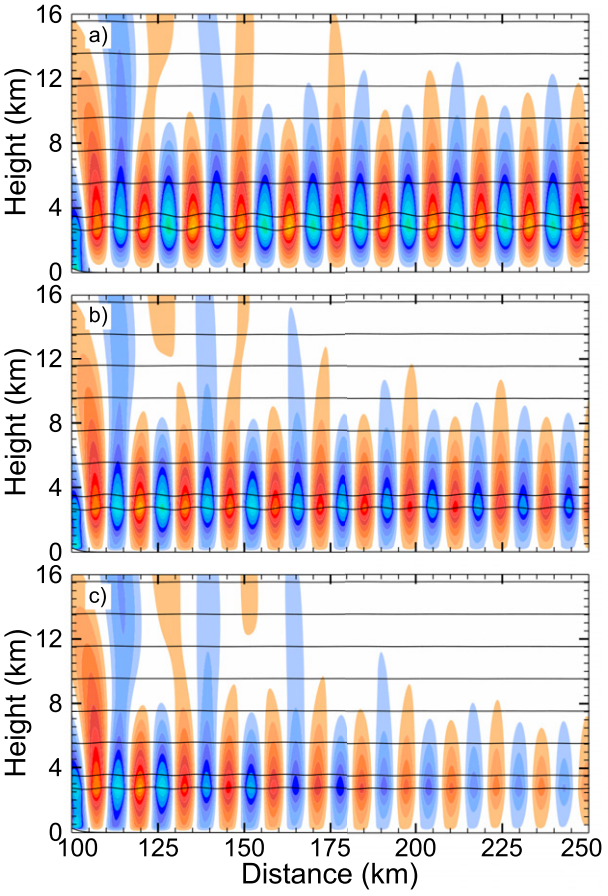

FIG. 9. Cross section of the normalized vertical velocity (color fill; 0.1 intervals; no fill for $-0.1 < w < 0.1\,\mathrm{m\,s}^{-1}$) and isentropes of potential temperature (black; 6-K interval) for profile 3b with no stratosphere: (a) free slip, (b) $z_0 = 0.0001$ m, and (c) $z_0 = 0.1$ m.

The influence of surface friction in the absence of a stratosphere is shown in Fig. 9. The resonant wavelength reduces from 13.9 km in the free-slip case (Fig. 9a) to 13.1 km when $z_0 = 0.0001$ m (Fig. 9b) and to 13.0 km when $z_0 = 0.1$ m (Fig. 9c). The downstream decay induced by surface friction is just slightly less than that produced by the same values of z_0 in profile 3a. When $z_0 = 0.1$ m, the waves 150 km downstream of the crest retain approximately 20% of their initial amplitude.

The preceding simulations were repeated with a tropopause at $z_T = 10$ km, with $N_s = 0.02\,\mathrm{s}^{-1}$ above. In the free-slip case (Fig. 10a), the downstream decay rate is 8.6% per wavelength, a value slightly smaller than the 10.8% per wavelength produced solely by surface friction when $z_0 = 0.1$ m and no stratosphere is present (Fig. 9c). As was the case in profile 3a, the downstream

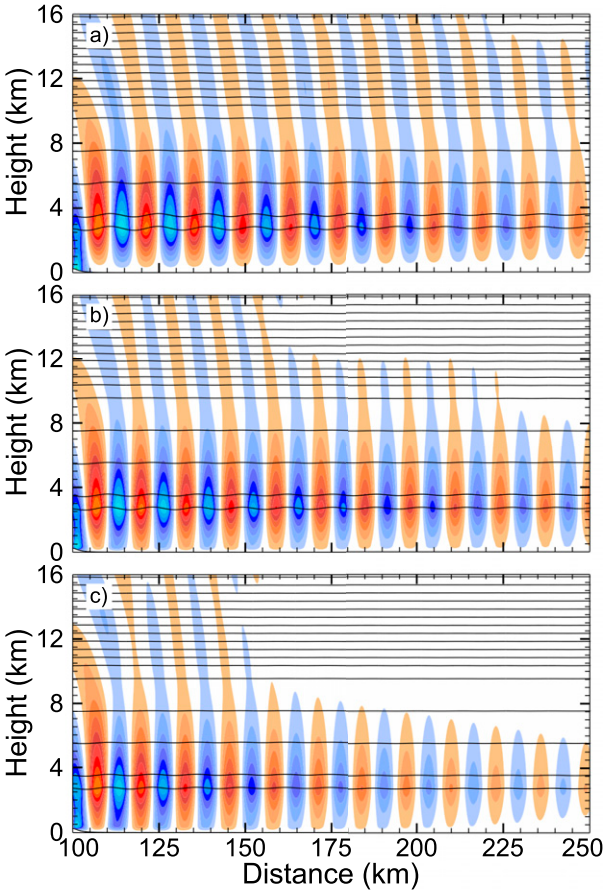

FIG. 10. As in Fig. 9, but for profile 3b with $z_T = 10$ km: (a) free slip, (b) $z_0 = 0.0001$ m, and (c) $z_0 = 0.1$ m.

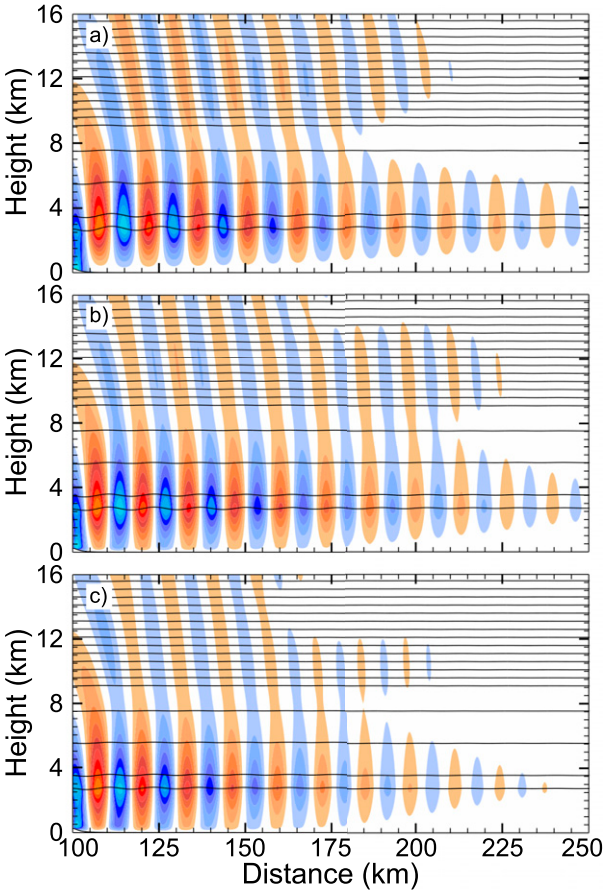

FIG. 11. As in Fig. 9, but for profile 3b with $z_T = 9$ km: (a) free slip, (b) $z_0 = 0.0001$ m, and (c) $z_0 = 0.1$ m.

decay in the presence of a stratosphere when $z_0 = 0.0001$ m (Fig. 10b) is weaker than in the free-slip case, albeit just slightly so. Again, this occurs because the reduction in upward leakage through the stratosphere (from the slight reduction in resonant wavelength and concomitant reduction in the penetration of the waves up to the tropopause) is more significant than the downstream decay produced directly by frictional losses. The most rapid downstream decay, amounting to a 13.5% loss per wavelength, is generated by the combined effects of stratospheric leakage and surface friction with $z_0 = 0.1$ m (Fig. 10c).

DHB15 noted that the rate of upward leakage into the stratosphere is sensitive to the height of the tropopause. Lower tropopauses tend to produce more rapid downstream decay by allowing higher-amplitude waves to reach the stratosphere. Figure 11 shows the vertical velocity field for the same cases considered in Fig. 10, except that z_T is lowered from 10 to 9 km, which increases the resonant wavelength slightly to 14.4 km and roughly doubles the decay rate in the free-slip case to 16.6% per wavelength (Fig. 11a). In contrast to the situations shown in Fig. 6e and Fig. 10b, with the lower tropopause, the combined influence of upward leakage and weak surface friction ($z_0 = 0.0001$ m, Fig. 11b) gives very slightly stronger downstream decay than that produced by the stratosphere alone without any surface friction (the difference is less than 1% per wavelength). The most rapid decay is evident in Fig. 11c, where $z_0 = 0.1$ m.

In summary, for profile 3b the isolated effect of strong surface friction ($z_0 = 0.1$ m, Fig. 9c) produces modestly stronger decay than the isolated effect of stratospheric leakage when $z_T = 10$ km (Fig. 10a). Reducing z_T to 9 km, however, makes stratospheric leakage a distinctly more effective agent for downstream decay than surface friction.

5. Conclusions

The relative influence of stratospheric leakage and boundary layer dissipation on the downstream decay of

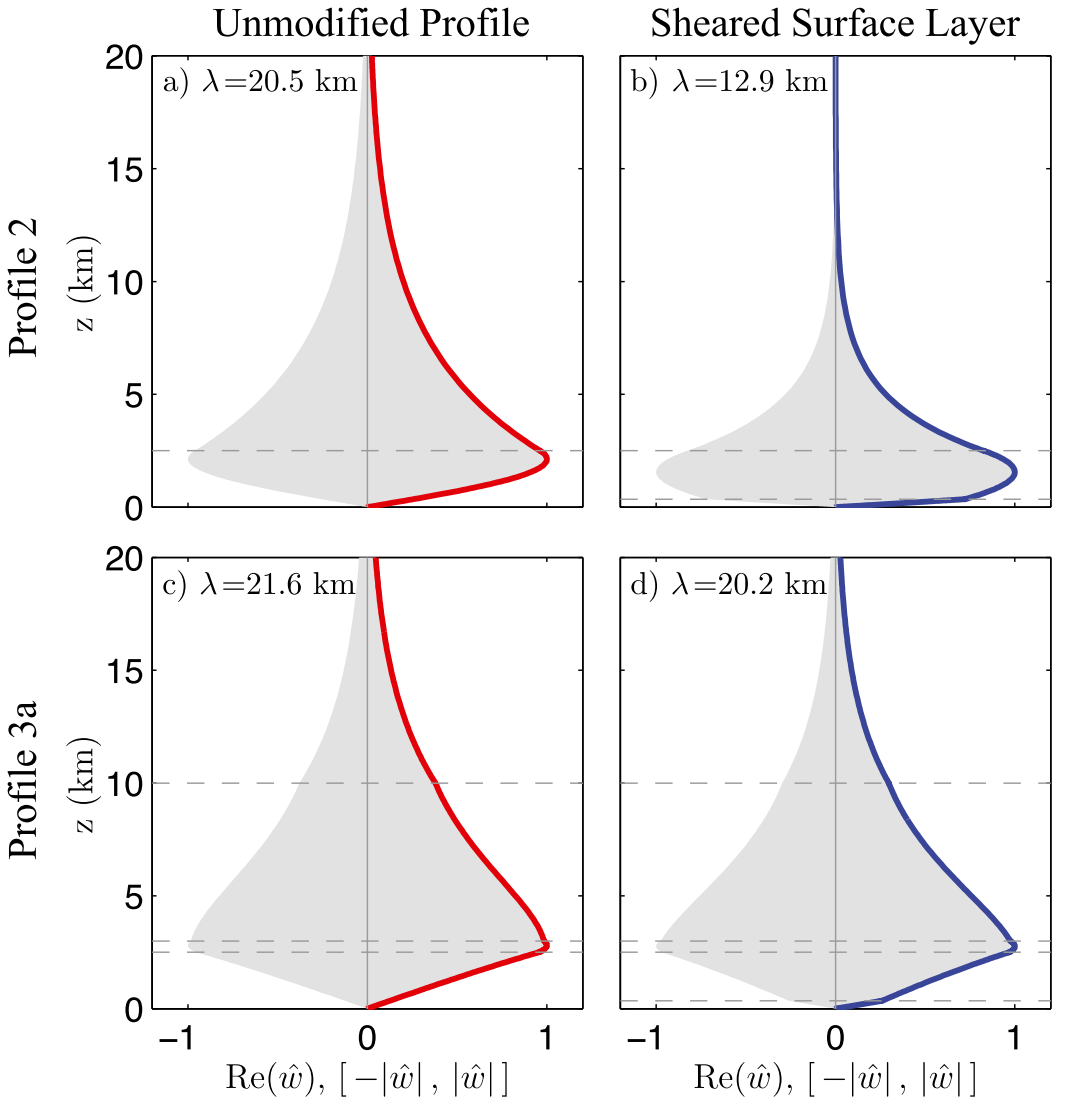

FIG. 12. Vertical structure of the vertical velocity Re[$\hat{w}(z)$] (colored lines; shading shows [$-|\hat{w}|$, $|\hat{w}|$]) of the trapped waves computed using the linear model in DHB15 for (a) the profile-2 mean state and (b) the profile-2 mean state modified to include a sheared surface layer. (c),(d) As in (a) and (b), but for profile 3a. The resonant wavelength λ is also noted.

trapped lee waves was examined for four different atmospheric profiles. In the highly idealized profiles 1 and 2, the wind speed is constant with height, the tropospheric stability has a simple two-layer structure, and stratospheric leakage had negligible influence whenever surface friction was present. The short 9.3-km-wavelength mode supported by profile 1 damps so rapidly with height throughout the upper troposphere that, even in free-slip simulations, stratospheric leakage produces only minimal downstream decay. The 20.8-km resonant wavelength for profile 2 is much longer, and this mode does undergo significant decay through stratospheric leakage in free-slip simulations. But when even weak surface friction is present, both the resonant wavelength and the vertical penetration of the waves into the upper troposphere are drastically reduced (to 12.8 km when $z_0 = 0.0001$ m), and stratospheric leakage becomes unimportant.

The situation is quite different for profiles 3a and 3b, for which leakage into the stratosphere is a significant downstream decay mechanism in both the free-slip and surface-friction simulations. These profiles, with elevated inversions and winds that increase with height, are much more typical of conditions observed during trapped-lee-wave events than are profiles 1 and 2. Stratospheric leakage is more important than boundary

layer friction in dissipating the 21.8-km-wavelength waves supported by profile 3a, whereas both effects have roughly similar influence on the 13.9-km waves supported by profile 3b.

In contrast to profiles 1 and 2, neither the horizontal wavelengths nor the upward penetration of the trapped waves supported by profiles 3a and 3b are greatly influenced by surface friction, although there is a slight reduction in wavelength and vertical penetration that actually reduces the net downstream decay in some cases with weak surface friction. In particular, in both of these profiles, waves decay more slowly in the presence of a stratosphere at $z_T = 10$ km when free-slip conditions are replaced by a boundary layer with $z_0 = 0.0001$ m. Recalling that $z_0 = 0.0001$ m is a surface roughness characteristic of the ocean, these results support the idea that differences in surface friction are an important factor driving the general tendency, revealed in satellite imagery, of lee waves to extend farther downstream from their source over the oceans than over land.

The change in the resonant wavelength generated by surface friction arises primarily through the modification of the mean-state wind speed profile, a result that is consistent with the theoretical argument of Jiang et al. (2006) that trapped-wave absorption in the boundary layer has little direct influence on the resonant wavelength. When $z_0 = 0.0001$ m, the mean surface wind speed is modified to an approximately linear shear, from $5\,\mathrm{m\,s^{-1}}$ at the surface to the unmodified background wind speed at a height of 350 m. The influence of this low-level shear layer on the vertical velocity profile $\mathrm{Re}(\hat{w})$ and on the resonant wavelength λ of inviscid lee waves supported by profiles 2 and 3a, as computed using the linear eigenvalue solver in DHB15, is shown in Fig. 12. The differences in the resonant wavelengths obtained using the numerical model and the values from linear theory (noted in Fig. 12) are never greater than 2%. The low-level wind shear reduces λ to 63% of that for the unmodified profile 2. This reduction is facilitated by the large near-surface value of the static stability ($N = 0.016\,\mathrm{s^{-1}}$), which allows the modal structure to change rapidly where the near-surface winds are weak and substantially lowers the level of maximum w. In contrast, the low-level stability in profile 3a is much weaker ($N = 0.003\,\mathrm{s^{-1}}$). When the friction-induced shear layer is present, the level of maximum vertical velocity remains within the inversion layer, and the resonant wavelength is only reduced to 93.5% of that for the unmodified profile.

For a given surface roughness, the effectiveness with which stratospheric leakage produces downstream decay in trapped lee waves clearly depends on the details of the atmospheric structure. Our results suggest that stratospheric leakage will be relatively more important for waves trapped by forward wind shear in profiles where the low-level stability is concentrated in an elevated inversion than it would be for waves trapped only by stability changes in simple two-layer atmospheres with constant wind speeds. As emphasized in DHB15 and confirmed here for profile 3b, the height of the tropopause is another important factor modulating stratospheric leakage, with 1-km reductions in its elevation having the potential to greatly increase the downstream decay (c.f. Figs. 10, 11).

Understanding the roles of surface friction and stratospheric leakage in the decay of trapped waves is important for understanding the momentum budget of the atmosphere. When waves leak into the stratosphere, they exert a drag on the larger-scale flow in the elevated region in which they ultimately decay. In contrast, when waves decay through the influence of surface friction, this drag is exerted very near the surface. To obtain a complete understanding of the drag produced by trapped waves on the large-scale flow, our investigation could be extended to consider the influence of surface heat fluxes on the waves (Jiang et al. 2006) and to include other decay mechanisms, such as time-dependent changes in the background flow (Hills and Durran 2012) and three-dimensional dispersion from a horizontally compact source.

Acknowledgments. This research was supported by National Science Foundation Grant AGS-1138977. Computations were performed using the Extreme Science and Engineering Discovery Environment (XSEDE), which is supported by National Science Foundation Grant ACI-1053575. The manuscript was improved by comments from two anonymous reviewers.

APPENDIX A

Subgrid-Scale Mixing

To parameterize the effects of turbulence that occurs on scales smaller than we are resolving, the model uses a first-order closure scheme that depends upon the relative strengths of stratification and shear. Subgrid-scale effects are evaluated by their impact on the velocity field through terms D_u, D_v, and D_w. Assuming all y derivatives are zero, but retaining all three velocity components, the formulation of Lilly (1962) becomes

$$D_u = \frac{\partial}{\partial x}(K_M \Delta_{1,1}) + \frac{\partial}{\partial z}(K_M \Delta_{1,3}), \tag{A1}$$

$$D_v = \frac{\partial}{\partial x}(K_M \Delta_{1,2}) + \frac{\partial}{\partial z}(K_M \Delta_{2,3}), \quad \text{and} \tag{A2}$$

$$D_w = \frac{\partial}{\partial x}(K_M \Delta_{1,3}) + \frac{\partial}{\partial z}(K_M \Delta_{3,3}), \tag{A3}$$

where

$$\Delta_{1,1} = \frac{4}{3}\frac{\partial u}{\partial x} - \frac{2}{3}\frac{\partial w}{\partial z}, \quad \Delta_{2,2} = -\frac{2}{3}\left(\frac{\partial u}{\partial x} + \frac{\partial w}{\partial z}\right),$$
$$\Delta_{3,3} = \frac{4}{3}\frac{\partial w}{\partial z} - \frac{2}{3}\frac{\partial u}{\partial x}, \tag{A4}$$

$$\Delta_{1,2} = \frac{\partial v}{\partial x}, \quad \Delta_{2,3} = \frac{\partial v}{\partial z}, \quad \Delta_{1,3} = \frac{\partial u}{\partial z} + \frac{\partial w}{\partial x}, \tag{A5}$$

$$\mathscr{D}^2 = \frac{1}{2}(\Delta_{1,1}^2 + \Delta_{2,2}^2 + \Delta_{3,3}^2) + \Delta_{1,2}^2 + \Delta_{2,3}^2 + \Delta_{1,3}^2, \quad \text{and} \tag{A6}$$

$$K_M = (k\Delta z)^2 \mathscr{D} \times \left[\max\left(1 - \frac{K_H}{K_M}\mathrm{Ri}, 0\right)\right]^{1/2}, \tag{A7}$$

where $\mathrm{Ri} = N^2/\mathscr{D}^2$ is the Richardson number.

The impact of subgrid-scale mixing on the potential temperature is modeled as

$$D_\theta = \frac{\partial}{\partial x}\left(K_H \frac{\partial \theta}{\partial x}\right) + \frac{\partial}{\partial z}\left(K_H \frac{\partial \theta}{\partial z}\right). \tag{A8}$$

We use $k = 0.21$ (Deardorff 1971) and $K_H/K_M = 3$ (Deardorff 1972). This ratio means that turbulent mixing begins when Ri drops below $\frac{1}{3}$, which is slightly larger than the typical critical value for the stability of a shear flow, Ri = 0.25.

APPENDIX B

Boundary Layer Parameterization

Our simulations use a boundary layer parameterization that is a simplified version of Blackadar's first-order closure scheme (Zhang and Anthes 1982). A surface level z_s is added at a fixed height of 10 m, at which three 2D variables (u_s, v_s, and θ_s) are evaluated to represent the surface conditions. The parameterization contains no surface heat flux, as the surface temperature is set to equal the air temperature at z_s. Additionally, the parameterization is restricted to situations with either a neutral or stably stratified boundary layer—assumptions in agreement with the profiles used in the current study.

In this work, boundary layer drag is made stronger by increasing surface friction as the roughness length z_0 is increased. The roughness length impacts the model equations through the friction velocity u_* and the surface stress τ_s:

$$u_* = \frac{\kappa |\mathbf{u}_s|}{\ln(z_s/z_0)} \quad \text{and} \tag{B1}$$

$$\tau_s = \rho u_*^2, \tag{B2}$$

where $\kappa = 0.4$ is von Kármán's constant.

The static stability in the lowest levels N_s is evaluated between z_s and the lowest regular grid level. An eddy diffusivity K_{H_s} is also evaluated between these levels, with Δz set to 40 m. Finally, the three surface variables are integrated forward in time using a trapezoidal scheme shown here (where the subscript 1 indicates values on the first regular grid level at height $\Delta z/2$):

$$\frac{\partial u_s}{\partial t} = \frac{K_{H_s}\dfrac{u_1 - u_s}{z_1 - z_s} - \dfrac{\tau_s}{\rho}\dfrac{u_s}{|\mathbf{u}_s|}}{\dfrac{1}{2}(z_1 - z_s)}, \tag{B3}$$

$$\frac{\partial v_s}{\partial t} = \frac{K_{H_s}\dfrac{v_1 - v_s}{z_1 - z_s} - \dfrac{\tau_s}{\rho}\dfrac{v_s}{|\mathbf{u}_s|}}{\dfrac{1}{2}(z_1 - z_s)}, \quad \text{and} \tag{B4}$$

$$\frac{\partial \theta_s}{\partial t} = \frac{K_{H_s}\dfrac{\theta_1 - \theta_s}{z_1 - z_s}}{\dfrac{1}{2}(z_1 - z_s)}. \tag{B5}$$

REFERENCES

Bougeault, P., 1983: A non-reflective upper boundary condition for limited-height hydrostatic models. *Mon. Wea. Rev.*, **111**, 420–429, doi:10.1175/1520-0493(1983)111<0420:ANRUBC>2.0.CO;2.

Bretherton, F. P., 1969: Momentum transport by gravity waves. *Quart. J. Roy. Meteor. Soc.*, **95**, 213–243, doi:10.1002/qj.49709540402.

Broad, A. S., 2002: Momentum flux due to trapped waves forced by mountains. *Quart. J. Roy. Meteor. Soc.*, **128**, 2167–2173, doi:10.1256/003590002320603593.

Brown, P. R. A., 1983: Aircraft measurements of mountain waves and their associated momentum flux over the British Isles. *Quart. J. Roy. Meteor. Soc.*, **109**, 849–865, doi:10.1002/qj.49710946211.

Deardorff, J. W., 1971: On the magnitude of the subgrid scale eddy coefficient. *J. Comput. Phys.*, **7**, 120–133, doi:10.1016/0021-9991(71)90053-2.

——, 1972: Numerical investigation of neutral and unstable planetary boundary layers. *J. Atmos. Sci.*, **29**, 91–115, doi:10.1175/1520-0469(1972)029<0091:NIONAU>2.0.CO;2.

Doyle, J., and D. Durran, 2002: The dynamics of mountain-wave induced rotors. *J. Atmos. Sci.*, **59**, 186–201, doi:10.1175/1520-0469(2002)059<0186:TDOMWI>2.0.CO;2.

Durran, D. R., 1995: Do breaking mountain waves decelerate the local mean flow? *J. Atmos. Sci.*, **52**, 4010–4032, doi:10.1175/1520-0469(1995)052<4010:DBMWDT>2.0.CO;2.

——, and J. B. Klemp, 1983: A compressible model for the simulation of moist mountain waves. *Mon. Wea. Rev.*,

111, 2341–2361, doi:10.1175/1520-0493(1983)111<2341:ACMFTS>2.0.CO;2.

——, M. O. G. Hills, and P. N. Blossey, 2015: The dissipation of trapped lee waves. Part I: Leakage of inviscid waves into the stratosphere. *J. Atmos. Sci.*, **72**, 1569–1584, doi:10.1175/JAS-D-14-0238.1.

Gaberšek, S., and D. R. Durran, 2006: Gap flows through idealized topography. Part II: Effects of rotation and surface friction. *J. Atmos. Sci.*, **63**, 2720–2739, doi:10.1175/JAS3786.1.

Georgelin, M., and F. Lott, 2001: On the transfer of momentum by trapped lee waves: Case of the IOP 3 of PYREX. *J. Atmos. Sci.*, **58**, 3563–3580, doi:10.1175/1520-0469(2001)058<3563:OTTOMB>2.0.CO;2.

Hills, M. O. G., and D. R. Durran, 2012: Nonstationary trapped lee waves generated by the passage of an isolated jet. *J. Atmos. Sci.*, **69**, 3040–3059, doi:10.1175/JAS-D-12-047.1.

——, and ——, 2014: Quantifying moisture perturbations leading to stacked lenticular clouds. *Quart. J. Roy. Meteor. Soc.*, **140**, 2013–2016, doi:10.1002/qj.2272.

Jiang, Q., J. D. Doyle, and R. B. Smith, 2006: Interaction between trapped waves and boundary layers. *J. Atmos. Sci.*, **63**, 617–633, doi:10.1175/JAS3640.1.

Klemp, J. B., and D. R. Durran, 1983: An upper boundary condition permitting internal gravity wave radiation in numerical mesoscale models. *Mon. Wea. Rev.*, **111**, 430–444, doi:10.1175/1520-0493(1983)111<0430:AUBCPI>2.0.CO;2.

Lilly, D. K., 1962: On the numerical simulation of buoyant convection. *Tellus*, **14A**, 148–172, doi:10.1111/j.2153-3490.1962.tb00128.x.

Ralph, F. M., P. J. Neiman, T. L. Keller, D. Levinson, and L. Fedor, 1997: Observations, simulations, and analysis of nonstationary trapped lee waves. *J. Atmos. Sci.*, **54**, 1308–1333, doi:10.1175/1520-0469(1997)054<1308:OSAAON>2.0.CO;2.

Shutts, G. J., 1992: Observations and numerical model simulation of a partially trapped lee wave over the Welsh mountains. *Mon. Wea. Rev.*, **120**, 2056–2066, doi:10.1175/1520-0493(1992)120<2056:OANMSO>2.0.CO;2.

Smith, R. B., S. Skubis, J. D. Doyle, A. S. Broad, C. Kiemle, and H. Volkert, 2002: Mountain waves over Mont Blanc: Influence of a stagnant boundary layer. *J. Atmos. Sci.*, **59**, 2073–2092, doi:10.1175/1520-0469(2002)059<2073:MWOMBI>2.0.CO;2.

——, Q. Jiang, and J. D. Doyle, 2006: A theory of gravity wave absorption by a boundary layer. *J. Atmos. Sci.*, **63**, 774–781, doi:10.1175/JAS3631.1.

Stiperski, I., and V. Grubišić, 2011: Trapped lee wave interference in the presence of surface friction. *J. Atmos. Sci.*, **68**, 918–936, doi:10.1175/2010JAS3495.1.

Teixeira, M. A. C., J. L. Argaín, and P. M. A. Miranda, 2013: Orographic drag associated with lee waves trapped at an inversion. *J. Atmos. Sci.*, **70**, 2930–2947, doi:10.1175/JAS-D-12-0350.1.

Vergeiner, I., 1971: An operational linear lee wave model for arbitrary basic flow and two-dimensional topography. *Quart. J. Roy. Meteor. Soc.*, **97**, 30–60, doi:10.1002/qj.49709741104.

Wieringa, J., 1992: Updating the Davenport roughness classification. *J. Wind Eng. Ind. Aerodyn.*, **41**, 357–368, doi:10.1016/0167-6105(92)90434-C.

Zhang, D., and R. A. Anthes, 1982: A high-resolution model of the planetary boundary layer—Sensitivity tests and comparisons with SESAME-79 data. *J. Appl. Meteor.*, **21**, 1594–1609, doi:10.1175/1520-0450(1982)021<1594:AHRMOT>2.0.CO;2.